RESEARCH ACTIVITIES II
Department of Molecular Structure

II-A Development of Dynamic Near-Field Spectroscopy and Application to Nanometric Systems

There is much demand for the study of local optical properties of molecular assemblies and materials, to understand mesoscopic phenomena and/or to construct optoelectronic devices in the nanometric scale. Scanning near-field optical microscopy (SNOM), which enables spatial resolution beyond the diffraction limit of light, showed remarkable progress in technology in the past decade. Combination of this advanced optical technology with ultrafast/nonlinear spectroscopic methods may offer a direct probe of molecular dynamical processes in mesoscopic systems. It may bring essential and basic knowledge for analyzing origins of characteristic features and functionalities of mesoscopic systems. We have constructed apparatuses for near-field dynamic spectroscopy with the femtosecond temporal resolution and the nanometer spatial resolution. Using the apparatuses developed, we are observing the characteristic spatiotemporal behavior of various organic molecular systems and metal nanoparticles, for the purpose of understanding spatial coherence and dissipation of excitations, and their dynamics. We also investigate experimentally the basic characteristics of near-field microscopic measurements. Outlines of the experimental results obtained are summarized here.

II-A-1 Photoluminescence from Gold Nanoplates Induced by Near-Field Two-Photon Absorption

IMURA, Kohei; NAGAHARA, Tetsuhiko; OKAMOTO, Hiromi

[*Appl. Phys. Lett.* **88**, 023104 (2006)]

We have investigated two-photon-induced photoluminescence (TPI-PL) properties of single gold nanoplates by using an apertured scanning near-field optical microscope. We found the remarkably large cross sections of TPI-PL from the gold nanoplates. It is one or two orders of magnitudes larger than those observed from the gold nanorods. The near-field PL images show characteristic spatial features. These PL images are in good agreement with the calculated spatial distribution of the electric fields adjacent to the particles at the excitation wavelength. We attribute the observed images to spatial characteristics of plasmon-mode wavefunctions. The TPI-PL images of the gold triangles are strongly dependent on the incident polarization and wavelength. We also found that the plasmon-mode excitation is the primary factor for enhancing the TPI-PL process. The result suggests that it would be possible to further improve the efficiency of TPI-PL by synthesizing the nanoparticles of controlled size and shape.

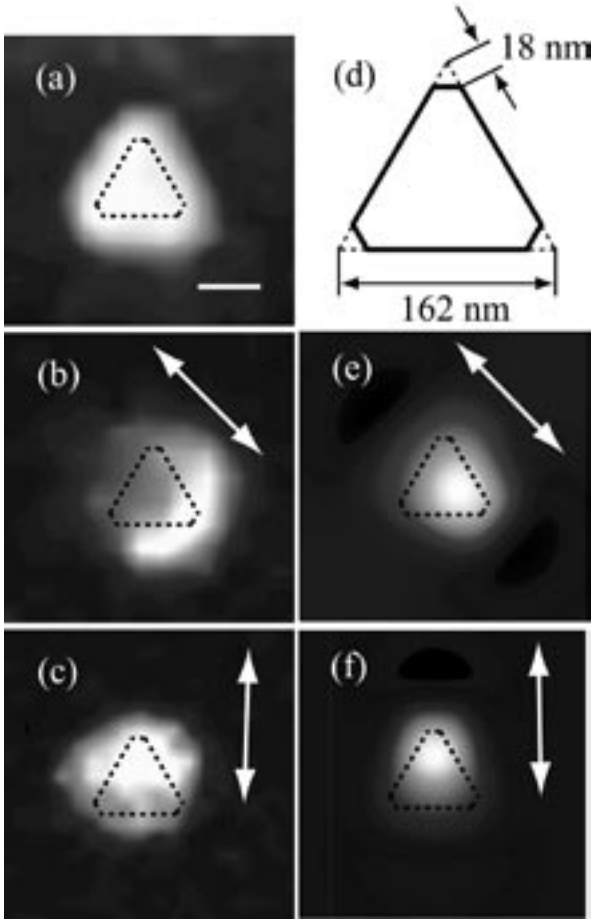

Figure 1. (a) Topography of a single gold triangle. (b), (c) Observed incident-polarization dependent TPI-PL images of the single gold triangle. (d) Schematic drawing of a snipped triangle used for calculations (e), (f). (e), (f) Calculated polarization-dependent electric field distributions near the snipped triangle. Arrows indicate the direction of the incident polarization. Dashed lines indicate approximate shape of the triangle. Scale bar: 100 nm.

II-A-2 Near-Field Imaging of SERS-Active Hot Spots on Metal-Nanoparticle Aggregates

IMURA, Kohei; OKAMOTO, Hiromi; HOSSAIN, Mohammad K.[1]; KITAJIMA, Masahiro[2]
([1]Univ. Tsukuba and NIMS; [2]NIMS, Univ. Tsukuba and IMS)

[*Chem. Lett.* **35**, 78–79 (2006)]

It is of fundamental importance to reveal the origin of the huge Raman enhancement in single-molecular level surface-enhanced Raman scattering. The major factor of the enhancement is considered to be an electromagnetic mechanism, *i.e.*, electric field enhancement induced by a plasmon resonance. For aggregated nanoparticles, strong electric field is expected in interstitial gaps between the nanoparticles ("hot spot"). Up to now, however, Raman enhancement on the hot spot site has not been directly shown by experiment. In this study, we succeeded in imaging of spatial distributions of electric-field enhancement and Raman-excitation probability for aggregates of gold nanospheres, using a scanning near-field optical microscope. To observe electric field enhancement, we used two-photon excitation probability imaging.[1)] The Raman excitation images were obtained by monitoring Raman band intensities while exciting the samples by cw lasers through the near-field fiber probe.

Figure 1 shows topographic, near-field two-photon excitation probability, and near-field Raman excitation probability (for dilutely doped dye molecule R6G) images, for aggregated gold nanospheres (diameter 100 nm). The two-photon image reflects spatial distribution of plasmon-induced electric field enhancement. The image shows that the aggregates, especially the gaps in the dimers, show strong electric field enhancements. Strong enhancements for the dimeric aggregates are also found in the Raman image. In contrast, the enhancements are not prominent in isolated particles. The present result gives a clear experimental proof to the theoretical prediction of hot spots.

Reference

1) K. Imura, T. Nagahara and H. Okamoto, *J. Phys. Chem. B* **109**, 13214 (2005).

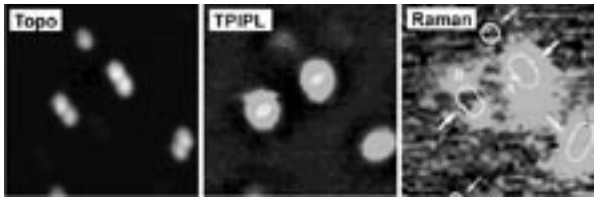

Figure 1. Topograph (left), near-field two-photon excitation (center), and near-field Raman excitation (right) images of gold nanospheres doped with R6G molecules. The Raman image was obtained for the R6G band at 1340 cm^{-1}. Image size: 1.5 μm × 1.5 μm.

II-A-3 Reciprocity in Scanning Near-Field Optical Microscopy: Illumination and Collection Modes of Transmission Measurements

IMURA, Kohei; OKAMOTO, Hiromi

[*Opt. Lett.* **31**, 1474–1476 (2006)]

There are two operational modes of near-field transmission experimental setup, *i.e.*, illumination (I) and collection (C) modes. In I-mode the object is illuminated through the near-field aperture probe, and the transmitted light is detected in the far field. In C-mode the object is illuminated by the far-field radiation, and the transmitted light is collected by the near-field probe. The configurations of I- and C-modes are optically reciprocal to each other. However, in the near-field experiment the reciprocity is not apparent or trivial.

We experimentally investigated the reciprocity of near-field measurements between I- and C-modes. Near-field transmission images of single gold spheres and nanorods observed by the two modes are found to be equivalent to each other in the region from visible to near infrared. This result shows that reciprocity holds for the near-field scattering problems. We found that the conventional optical selection rule for far-field excitations does not apply not only under I-mode but also with C-mode arrangements. The possible origin of this observation might be the near-field probe. The existence of the near-field probe tip close to the nanorod may perturb the electric field distribution near the gold nanorods. The local electric field generated in the presence of the near-field probe would allow SP-mode excitation at the tip position.

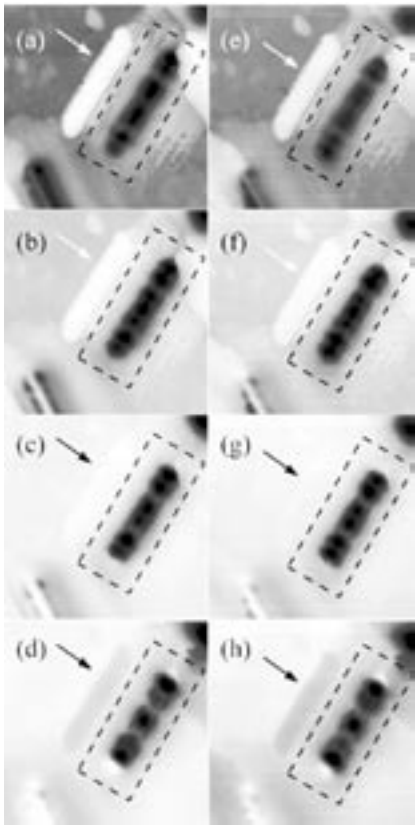

Figure 1. Transmission near-field optical images of a single gold nanorod (diameter 22±3 nm, length 510±30 nm): (a-d) I-mode, (e-h) C-mode. The scan area is 1 μm × 1 μm. Observed spectral region: (a,e) 607–627 nm, (b,f) 647–666 nm, (c,g) 666–686 nm, (d,h) 705–725 nm. Arrows indicate *z*-motion artifacts.

II-A-4 Near-Field Raman Study on the Close-Packed 2D Nanostructures of Gold Nanoparticles

HOSSAIN, Mohammad K.[1]; SHIMADA, Toru[2]; KITAJIMA, Masahiro[3]; IMURA, Kohei; OKAMOTO, Hiromi
([1]NIMS and Univ. Tsukuba; [2]NIMS; [3]NIMS, Univ. Tsukuba and IMS)

Metallic nanostructure, particularly gold nanostructure is an indispensable candidate for future nanoscale science and technology for its unique properties. We have studied electromagnetic field enhancement with surface-enhanced Raman scattering (SERS) and near-field spectroscopy for well-ordered two-dimensional (2D) nanostructures of gold nanoparticles. 2D nanostructures of gold nanoparticles (diameter 100 nm) were fabricated from gold colloids without using capping reagent or surfactant on glass substrate. The individual gold nanoparticles of the 2D structure were not in contact. The over all 2D structure area ranged from several 100 μm^2 to mm^2. Crystal violet (CV) or rhodamine 6G (R6G) molecules were dispersed on this 2D structure by spin-coating method.

The microscopic SERS spectrum of the adsorbed molecules on this Au 2D surface were measured. Several distinguishing peaks confirmed that such substrate was indeed SERS-active. The enhancement was highest at the edge of the 2D nanostructure.[1)] To exploit the spatial distributions of electromagnetic enhancement, scanning near-field optical measurement was performed for this 2D nanostructure. The Raman signal was enhanced at the 2D nanostructure of gold nanoparticles, especially along the edge of the 2D structure.

Reference

1) M. K. Hossain, K. Shibamoto, K. Ishioka, M. Kitajima, T. Mitani and S. Nakashima, *J. Lumin.* **122-123**, 792 (2006).

II-A-5 Enhancement and Quenching of Fluorescence from Dye Molecules by Single Gold Nanoparticles

HORIMOTO, Noriko N.; IMURA, Kohei; OKAMOTO, Hiromi

We investigated the enhancement and quenching of fluorescence from dye molecules by single gold nanoparticles, and their dependence on particle shape and size, using an aperture-type scanning near-field optical microscope. Gold nanoplates (thickness ~ 20 nm) showed large enhancements, and gold nanospheres (diameter ~ 30–100 nm) showed a moderate enhancement. On the other hand, gold nanorods (diameter ~ 20–40 nm, length ~ 100–500 nm) showed quenching. The enhancement and quenching mechanism is discussed based on electromagnetic effects.

II-A-6 Near-Field Two-Photon-Induced Photoluminescence from Single Gold Nanorods

IMURA, Kohei; OKAMOTO, Hiromi

We investigated photoluminescence (PL) properties of single gold nanorods (diameter 20–32 nm, length 190–630 nm) by using a near-field two-photon microscope. A PL spectrum of a single gold nanorod shows two peak wavelengths. The peaks are always observed near 550 nm and 650 nm, regardless the rod dimensions and plasmon modes excited. The intensity ratio (I_{650nm}/I_{550nm}) of the two spectral components varies with the rod dimension, and becomes nearly zero in the spherical particle limit. The results indicate that the PL appeared in the longer wavelength (~650 nm) gains the intensity in resonance with the longitudinal plasmon mode. The spectral features as well as polarization characters of the PL indicate that the emission process is dominantly occurred though a radiative recombination of an electron-hole pair generated by the two-photon excitation.

II-A-7 Ultrafast Near-Field Transient Imaging of Single Gold Nanorods

IMURA, Kohei; OKAMOTO, Hiromi

We investigated ultrafast transient behaviors in single nanorods (diameter 30 nm, length 300–330 nm) after an optical excitation with a 50-nm spatial resolution and a 100-fs time resolution. We used a near-infrared pulse to excite longitudinal plasmon resonances of the nanorod. Spatial patterns of transient images of the single nanorods observed at 1 ps delay time were similar to those of plasmon wavefunctions found in the steady-state transmission measurements (Figure 1).[1)] However, depending on the rod dimension, the image shows either induced absorptions or absorption bleaches at end edges of the nanorod.

To get a deeper understanding for the observed features of the transient transmission images, we simulated position-dependent transient transmission change by assuming that the photoexcitation induces a homogeneous electronic temperature rise in the nanorod. In the simulation, the transient transmission change at a position was considered to be proportional to the change of the electromagnetic local density-of-states (LDOS) due to the elevation of electronic temperature. The change of LDOS was evaluated by taking the temperature dependency of the dielectric constants of the gold into account. Simulated transient images qualitatively reproduced the observations. The observed transient images were thus assignable to the change of the LDOS due to the electronic temperature rise.

Reference

1) K. Imura, T. Nagahara and H. Okamoto, *J. Phys. Chem. B* **108**, 16344 (2004).

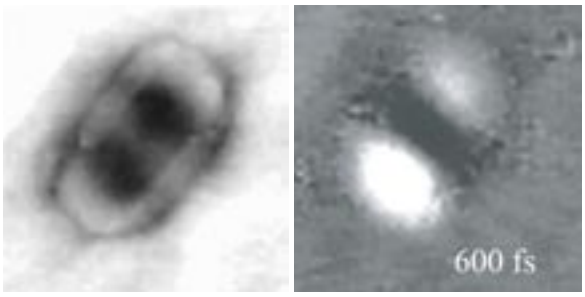

Figure 1. Typical near-field static transmission (left) and transient transmission change (right) images of gold nanorod (diameter 30 nm, length 300 nm). In the right panel, bleached and induced extinctions are indicated, respectively, in black and white.

II-A-8 Scanning Near-Field Optical Microscopic Study of Porphyrin Nanowire

NAGAHARA, Tetsuhiko; IMURA, Kohei; OKAMOTO, Hiromi; OZAWA, Hiroaki; OGAWA, Takuji

We studied optical properties of molecular nanowires of coupled zinc porphyrins with bulky dendric groups, by means of scanning near-field optical microscopy and spectroscopy. The topographic images and the near-field-excited fluorescence images gave string-like structures, and correlated well to each other. We also performed polarization dependence measurements. From the result of the analysis, it has been suggested that the photoexcitation is spatially propagated along the chain for appreciably long distance.

II-B Development of a Novel Solid-State NMR Technique

In order to alleviate an adversary effect of heating problem by irradiation of strong rf field for long duration, a novel solid state NMR technique has been explored as a means useful for a cross-polarization and separated local field NMR which enable to enhance sensitivity and determine relative orientation of the principal axes of the chemical shift and the heteronuclear dipolar interaction tensors, respectively. In the conventional approach, however, continuous rf irradiation of millisecond long rather than microsecond pulse used for conventional NMR is required. We have successfully developed a novel technique using weak rf fields without any serious loss of spectral quality. Therefore, this approach is essential for a study on biologically important molecules near under physiological conditions.

II-B-1 Remarkable Reduction of RF Power by ATANSEMA and DATANSEMA Separated Local Field in Solid-State NMR Spectroscopy

NISHIMURA, Katsuyuki; NAITO, Akira[1]
([1]Yokohama Natl. Univ.)

[*Chem. Phys. Lett.* **419**, 120–124 (2006)]

We proposed a novel approach to markedly reduce rf power for both ^{1}H and observed nuclei during spin exchange for separated local field experiments. The rf power to satisfy the Hartmann-Hahn matching conditions during spin exchange for observed nuclei was arbitrarily reduced by alternating the directions of effective fields for ^{1}H nuclei with unequal duration times and amplitudes. The proposed techniques were compared experimentally with those developed previously by the authors. The rf power for observed nuclei and average ^{1}H were reduced by factors of 9 and 2, respectively, for ^{13}C NMR signals of liquid crystalline 5CB.

References

1) K. Nishimura and A. Naito, *Chem. Phys. Lett.* **402**, 245–250 (2005).
2) C. H. Wu, A. Ramamoorthy and S. J. Opella, *J. Magn. Reson. A* **109**, 270–272 (1994).

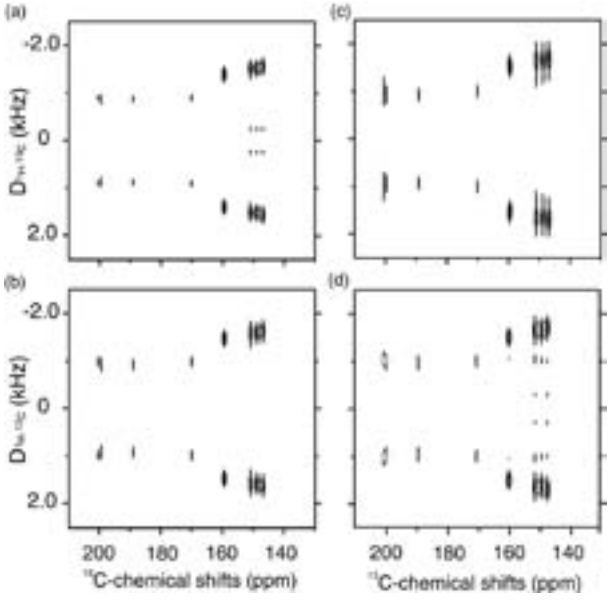

Figure 1. 2D-Separated local field ^{13}C-NMR spectra aromatic region of 5CB in the liquid crystalline state at 20 °C obtained by (a) TANSEMA[1)] (^{1}H, ^{13}C = 57.7, 11 W), (b) ATANSEMA ($^{1}H_{av}$, ^{13}C = 34.4, 11 W), (c) DATANSEMA ($^{1}H_{av}$, ^{13}C = 25.4 , 11 W), (d) PISEMA[2)] (^{1}H, ^{13}C = 57.7, 97 W).

II-B-2 Reduction of RF Power by Duration and Amplitude Time-Averaged Nutation Cross Polarization in Solid State NMR Spectroscopy

NISHIMURA, Katsuyuki; NAITO, Akira[1]
([1]Yokohama Natl. Univ.)

We have developed a new approach to markedly reduce rf power for both ^{1}H and observed nuclei during cross-polarization under static condition. The rf power to satisfy the Hartmann-Hahn matching condition for observed nuclei was arbitrary reduced by alternating the direction of effective fields with unequal-duration times and -amplitudes. The proposed technique was compared theoretically and experimentally with the previously developed duration time averaged technique with and without ^{1}H-homonuclear dipolar decoupling. The rf power for observed nuclei and averaged power for ^{1}H were shown to be reduced experimentally by factors of 9 and 2, respectively, as manifested from ^{13}C-NMR signals of MBBA in the liquid crystalline state without expense of reduced signals.

References

1) K. Nishimura and A. Naito, *Chem. Phys. Lett.* **380**, 569–576 (2003).
2) R. K. Hester, J. L. Ackerman, V. R. Cross and J. S. Waugh, *Phys. Rev. Lett.* **34**, 993–995 (1975).

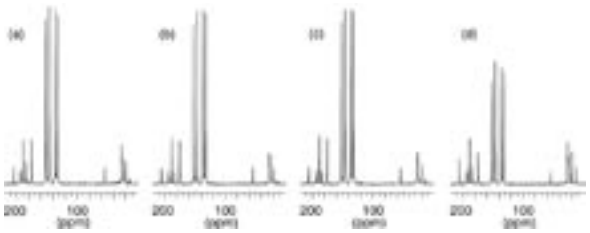

Figure 1. ^{13}C-NMR spectra of MBBA in the liquid crystalline state at 20 °C obtained by (a) TANMA-CP[1)] (^{1}H, ^{13}C = 57.7, 11 W), (b) ATANMA-CP ($^{1}H_{av}$, ^{13}C = 34.4, 11 W), (c) DATANMA-CP ($^{1}H_{av}$, ^{13}C = 25.4, 11 W), and (d) LG-CP[2)] (^{1}H, ^{13}C = 57.7, 97 W).

II-C Structural Characterization of Biomolecules by Solid State NMR

Solid state NMR is an excellent technique to examine structures and dynamics of biomolecules including membrane proteins or membrane-associated peptides at physiological temperature. In particular, we have explored to reveal the functional role of membrane proteins or peptides inside or at the membrane surface of fully hydrated lipid bilayers by using solid state NMR at ambient temperature.

II-C-1 Histidines, Heart of the Hydrogen Ion Channel from Influenza A Virus: Toward an Understanding of Conductance and Proton Selectivity

HU, Jun[1]; FU, Riqiang[1]; NISHIMURA, Katsuyuki; ZHANG, Li[1]; ZHOU, Huan-Xiang[1]; BUSATH, David D.[2]; VIJAYYERGIYA, Viksita[2]; CROSS, Timothy A.[1]
([1]Florida State Univ. and Natl. High Magnetic Field Laboraory; [2]Brigham Young Univ.)

[*Proc. Natl. Acad. Sci. U.S.A.* **103**, 6865–6870 (2006)]

The heart of the H^+ conductance mechanism in the homotetrameric M2 H^+ channel from influenza A is a set of four histidine side chains. Here, we show that protonation of the third of these imidazoles coincides with acid activation of this transmembrane channel and that, at physiological pH, the channel is closed by two imidazole–imidazolium dimers, each sharing a low-barrier hydrogen bond. This unique construct succeeds in distributing a pair of charges over four rings and many atoms in a low dielectric environment to minimize charge repulsion. These dimers form with identical pK_{as} of 8.2±0.2, suggesting cooperative H^+ binding and clearly illustrating high H^+ affinity for this channel. The protonation behavior of the histidine side chains has been characterized by using solid-state NMR spectroscopy on the M2 transmembrane domain in fully hydrated lipid bilayers where the tetrameric backbonestructure is known. Furthermore, electrophysiological measurements of multichannel and single-channel experiments confirm that these protein constructs are functional.

II-C-2 Conformational Changes of Adrenocorticotropic Hormone, ACTH (1-24), Bound to Lipid Bilayers, Dependent upon Proportion of Lipids Composition, as Studied by Solid State NMR

NISHIMURA, Katsuyuki; MYOGA, Hiroki[1]; NARITA, Muneto[1]; KIRA, Atsushi[2]; NAITO, Akira[1]
([1]Yokohama Natl. Univ.; [2]ULVAC Inc.)

Local conformations of ACTH (1-24), bound to fully hydrated multibilayers consisting of neutral and anionic lipids (DMPC/DMPG) at liquid crystalline, were examined by ^{13}C-solid state NMR. It turned out that ACTH (1-24) exhibited conformational changes depending upon the lipid composition of DMPC to DMPG. The binding constants of ACTH (1-24) to the lipid bilay ers were determined by a quartz crystal microbalance (QCM) for various DMPC/DMPG proportion. The local maximum was seen at the proportion of DMPG/(DMPC + DMPG) = 0.25, which is close to the composition of neutral and anionic lipids occurring in human cells. This result suggests that ACTH (1-24) has favorable lipid composition in order to bind tightly lipid bilayers pior to reach receptor, together with changing its conformation depending on the lipid composition.

II-D Structure and Function of Metalloproteins and Its Molecular Design

Metal ion is a common cofactor that is crucial for active centers of proteins involved in many biologically important processes in cells, and a relatively small number of metal-based prosthetic groups are utilized to serve numerous and diverse chemical functions. A typical metal-based prosthetic group, which represents a fascinating example in this respect, is heme. Heme promotes a variety of functions, such as dioxygen storage, activation of small molecules, electron transfer reactions, and sensing gaseous molecule. In the field of protein design and engineering, hemoproteins also make particularly attractive targets. There are many reasons for this, including the exciting possibility of engineering protein-based molecules with useful catalytic, electronic or optoelectronic properties. Based on various kinds of spectroscopies, we have functionally and structurally characterized some hemoproteins including newly identified heme-regulated proteins, and designed hemoproteins showing improved activities and new functions.

II-D-1 Absence of a Detectable Intermediate in the Compound I Formation of Horseradish Peroxidase at Ambient Temperature

SHINTAKU, Masato[1]; MATSUURA, Koji[1]; TAKAHASHI, Satoshi[1]; ISHIMORI, Koichiro[2]; MORISHIMA, Isao[1]
([1]Kyoto Univ.; [2]IMS and Kyoto Univ.)

[*J. Biol. Chem.* **280**, 40934–40938 (2005)]

A microsecond-resolved absorption spectrometer was developed to investigate the elementary steps in hydrogen peroxide (H_2O_2) activation reaction of horseradish peroxidase (HRP) at ambient temperature. The kinetic absorption spectra of HRP upon the mixing with various concentrations of H_2O_2 (0.5–3 mm) were monitored in the time range from 50 to 300 μs. The time-resolved spectra in the Soret region possessed isosbestic points that were close to those between the resting state and compound I. The kinetic changes in the Soret absorbance could be well fitted by a single exponential function. Accordingly, no distinct spectrum of the putative intermediate between the resting state and compound I was identified. These results were consistent with the proposal that the O–O bond activation in heme peroxidases is promoted by the imidazolium form of the distal histidine that exists only transiently. It was estimated that the rate constant for the breakage of the O–O bond in H_2O_2 by HRP is significantly faster than 1×10^4 s^{-1}.

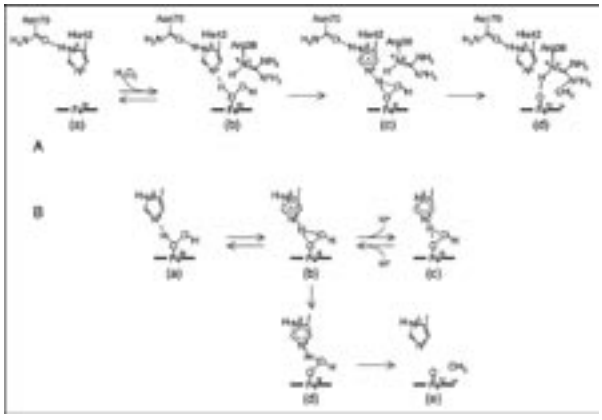

Figure 1. The proposed formation mechanisms of compound I. *A*, the formation mechanism of compound I in heme peroxidases proposed by Poulos and Kraut. The amino acid numbering is for HRP, although the original proposal was based on the structure of cytochrome *c* peroxidase. *(a)*, the resting state. *(b)* and *(c)*, the hypothetical intermediate and transition state structures for the compound I formation. His-42 acts as a general acid-base catalyst and translocates a proton from the proximal to the distal oxygen. *(d)*, compound I. The hydrogen bonds between oxygen atoms and Arg-38 were detected in the recent crystallographic data. *B*, the generalized mechanism of hydrogen peroxide activation by heme proteins described by Egawa *et al. (a)*, the hydrogen peroxide-bound form. *(b)*, the transition state for the O–O bond heterolysis. The structure is unstable because of the doubly protonated His. *(c)*, the deprotonation of the distal His causes the stabilization of the iron hydroperoxide complex. *(d)*, the proton translocation occurs only from the structure (*(b)*). *(e)*, compound I.

II-D-2 Dehydration in the Folding of Reduced Cytochrome *c* Revealed by the Electron-Transfer-Triggered Folding under High Pressure

KIMURA, Tetsunari[1]; SAKAMOTO, Koichi[2]; MORISHIMA, Isao[1]; ISHIMORI, Koichiro[3]
([1]Kyoto Univ.; [2]Kyoto Univ. and Hokkaodo Univ.; [3]IMS, Kyoto Univ. and Hokkaodo Univ.)

[*J. Am. Chem. Soc*. **128**, 670–671 (2006)]

We determined the activation volume associated with protein folding of reduced cytochrome *c* from the collapsed intermediate to the native state. The folding rate was followed by a change in the absorption (420 nm) at various pressures between 0.1 and 200 MPa and at various concentrations of denaturant (guanidine hydrochloride) between 3.2 and 4.0 M. Dependence of the folding rate on both these factors revealed that the activation volume at ambient pressure in the absence of denaturant is negative ($\Delta V^{\ddagger} = -14 \pm 7$ $cm^3 \cdot mol^{-1}$). Such a negative activation volume can be accounted for by a decrease in volume resulting from the dehydration of hydrophobic groups, primarily the heme group. Dehydration, which increases the entropy of the protein system, compensates for a decrease in the entropy

accompanying the formation of the more compact and ordered transition state. We, therefore, propose that the positive change in the activation entropy for the folding reaction is due to the dehydration of hydrophobic groups. Furthermore, dehydration entropically promotes the protein folding reaction.

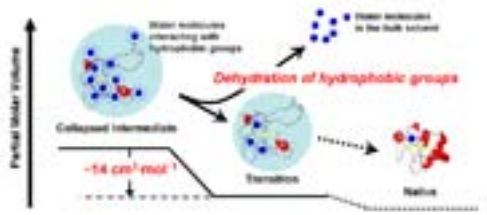

Figure 1. Volume profile for protein folding of cytochrome *c*.

II-D-3 Time-Resolved Small Angle X-Ray Scattering Investigation on the Folding Dynamics of Heme Oxygenase: Implication of the Scaling Relationship for the Submillisecond Intermediates of Protein Folding

UZAWA, Takanori[1]; KIMURA, Tetsunari[1]; ISHIMORI, Koichiro[2]; MORISHIMA, Isao[1]; MATSUI, Toshitaka[3]; IKEDA-SAITO, Masao[3]; TAKAHASHI, Satoshi[4]; AKIYAMA, Shuji[5]; FUJISAWA, Tetsuro[5]
([1]Kyoto Univ.; [2]IMS and Kyoto Univ.; [3]Tohoku Univ.; [4]Osaka Univ.; [5]RIKEN)

[*J. Mol. Biol.* **357**, 997–1008 (2006)]

Polypeptide collapse is generally observed as the initial folding dynamics of proteins with more than 100 residues, and is suggested to be caused by the coil-globule transition explained by Flory's theory of polymers. To support the suggestion by establishing a scaling behavior between radius of gyration (R_g) and chain length for the initial folding intermediates, the folding dynamics of heme oxygenase (HO) was characterized by time-resolved, small-angle X-ray scattering. HO is a highly helical protein without disulfide bridges, and is the largest protein (263 residues) characterized by the method. The folding process of HO was found to contain a transient oligomerization; however, the conformation within 10 ms was demonstrated to be monomeric and to possess R_g of 26.1±1.1 Å. Together with the corresponding data for proteins with different chain lengths, the seven R_g values demonstrated the scaling relationship to chain length with a scaling exponent of 0.35±0.11, which is close to the theoretical value of 1/3 predicted for globules in solutions where monomer-monomer interactions are favored over monomer-solvent interactions (poor solvent). The finding indicated that the initial folding dynamics of proteins bears the signature of the coil-globule transition, and offers a clue to explain the folding mechanisms of proteins with different chain lengths.

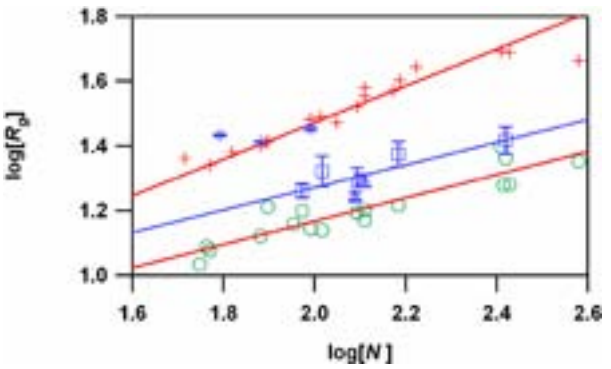

Figure 1. The correlation plots between R_g and chain length (N) for the chemically unfolded states (crosses), native states (circles) and initial collapsed intermediates (squares and triangles) of various proteins. Squares and triangles represent R_g values obtained with the submillisecond and millisecond time resolutions, respectively. Lines denote the scaling relationships for the respective states. The data for the chemically unfolded state, and for the native state, are reported elsewhere.

II-E Structure and Energy Changes during Protein Reaction Dynamics

The thermodynamic properties (enthalpy, thermal expansion coefficient, compressibility, partial molar volume, *etc*.) as well as the transport property (diffusion coefficient) of proteins are of fundamental importance to understand the structural fluctuation and the dynamics of protein molecules. Traditional techniques that can access to these quantities are certainly useful and powerful to characterize the proteins. However, knowledge of these properties of time-dependent or unstable (intermediate) species during biological reactions is very limited. It is most desirable to develop and use a method that can measure these properties in time domain so that reaction intermediates can be characterized in a similar way. In this project, we try to construct a method to probe energies and conformational changes as well as the diffusion coefficients of biological proteins in time domain. One of interesting applications of this technique is to detect spectral silent kinetics in reactions of biological proteins.

II-E-1 Time-Resolved Thermodynamics: Heat Capacity Change of Transient Species during Photo-Reaction of PYP

KHAN, Javaid Shahbaz[1]; IMAMOTO, Yasushi[3]; KATAOKA, Mikio[3]; TOKUNAGA, Fumio[4]; TERAZIMA, Masahide[2]
([1]Kyoto Univ.; [2]IMS and Kyoto Univ.; [3]Nara Inst. Sci. Tech.; [4]Osaka Univ.)

[*J. Am. Chem. Soc.* **128**, 1002–1008 (2006)]

Heat capacity changes of short lived transient species in different time ranges were measured for the first time by using the thermal component of the transient grating and transient lens signals at various temperatures. This method was applied to the transient intermediates of Photoactive Yellow Protein (PYP). The temperature dependence of the enthalpy change shows that the heat capacity of the short lived intermediate pR_2 (also called I_1 or PYP_L) species is the same as that of the ground state (pG) species within our experimental accuracy, whereas that of the long lived intermediate pB (I_2 or PYP_M) is much larger (2.7±0.4 kJ/mol K) than that of pG. The larger heat capacity is interpreted in terms of the conformational change of the pB species such as melted conformation and/or exposure of the non-polar residues to the aqueous phase. This technique can be used for photochemical reaction in general to investigate the conformational change and the hydrophobic interaction in time domain.

II-E-2 Conformational Changes of PYP Monitored by Diffusion Coefficient: Effect of N-Terminal α-Helices

KHAN, Javaid Shahbaz[1]; IMAMOTO, Yasushi[3]; HARIGAI, Miki[3]; KATAOKA, Mikio[3]; TERAZIMA, Masahide[2]
([1]Kyoto Univ.; [2]IMS and Kyoto Univ.; [3]Nara Inst. Sci. Tech.)

[*Biophys. J.* **90**, 3686–3693 (2006)]

Conformational changes in the light illuminated intermediate (pB) of photoactive yellow protein (PYP) were studied from a view point of the diffusion coefficient (D) change of several N-truncated PYPs, which lacked the N-terminal 6, 15, or 23 amino acid residues (T6, T15, and T23, respectively). For intact PYP (i-PYP), D of pB (D_{pB}) was *c.a.* 11% lower than that (D_{pG}) of the ground state (pG) species. The difference in D ($D_{pG} - D_{pB}$) decreased upon cleavage of the N-terminal region in the order of i-PYP > T6 > T15 > T23. This trend clearly showed that conformational change in the N-terminal group is the main reason for the slower diffusion of pB. This slower diffusion was interpreted in terms of the unfolding of the two α-helices in the N-terminal region, increasing the intermolecular interactions due to hydrogen bonding with water molecules. The increase in friction per one residue by the unfolding of the α-helix was estimated to be 0.3×10^{-12} kg/s. The conformational change in the N-terminal group upon photo-illumination is discussed.

II-E-3 Diffusion Coefficient and the Secondary Structure of Poly-L-Glutamic Acid in Aqueous Solution

INOUE, Keiichi[1]; BADEN, Naoki[1]; TERAZIMA, Masahide[2]
([1]Kyoto Univ.; [2]IMS and Kyoto Univ.)

[*J. Phys. Chem. B* **109**, 22623–22628 (2005)]

The diffusion coefficients (D) of poly-L-glutamic acid (PLG) at various pH were investigated by the laser induced transient grating method with a new photoreactive probe molecule. The pH dependence of D was compared with that of the helical content of PLG measured by the circular dichroism. It was found that the pH dependences of both quantities are very similar. Since the frictions of the translational diffusion of charged and protonated carboxyl group were found to be similar each other, it was concluded that the conformation of the main polymer chain is a main factor to determine the diffusion process; that is, the α-helix conformation makes the molecular diffusion faster. This result indicates that the conformational change of a protein can be detected by monitoring the diffusion coefficient.

II-F Surface Magnetism of Ultrathin Films: Search of New Phenomena and Exploitation of New Techniques

Noble properties of magnetic thin films such as perpendicular magnetic anisotropy (PMA) and giant magnetoresistance (GMR) have extremely attracted scientific and technological interests. The origin of perpendicular magnetic anisotropy of ultrathin metal films is not fully understood and is an important subject in fundamental physics but is useful for high-density recording media. The GMR property is already utilized for read-heads of hard disk drives, although quantitative understanding of the GMR is still to be improved.

Our research subjects are twofold. The first one is to find out new important phenomena concerning surface magnetism. We have been investigating drastic changes of magnetic properties of ultrathin metal films by using surface chemical modification such as atoms/molecules adsorption on the surface. This is studied by several sophisticated techniques such as the synchrotron radiation x-ray magnetic circular dichroism (XMCD), the visible-light magneto-optical Kerr effect (MOKE) and the magnetization induced second harmonic generation (MSHG) techniques. A goal of these works is spin engineering by which the magnetization of ultrathin metal films and nanowires can be controlled artificially.

The second one is to exploit new techniques for the investigations of surface magnetism. Last year we discovered surprising enhancements of the magnetic circular dichroism (MCD) in the threshold photoemission, which provide the possibility of the visible and ultraviolet (UV) MCD photoemission electron microscopy (PEEM).

II-F-1 Effect of Adsorbate Carbon on Spin Reorientation Transitions in Cu-Capped Ultrathin Ni Films on Cu(001)

NAKAGAWA, Takeshi; WATANABE, Hirokazu; YOKOYAMA, Toshihiko

[*Surf. Sci.* **599**, 262–269 (2005)]

We have reinvestigated the Cu capping effect for Ni films on clean Cu(001) by means of polar and longitudinal MOKE measurements in order to account for previous discrepancies[1,2] among the results regarding whether the Cu capping stabilizes perpendicular or in-plane magnetization. Figure 1(a) shows the Ni thickness dependence of the polar and longitudinal MOKE results of Ni/Cu(001) before and after Cu capping. The perpendicular magnetization from the polar MOKE appears at smaller thickness in Cu-capped Ni/Cu(001). We can immediately conclude that Cu capping stabilizes perpendicular magnetization.

We also found that the previous erroneous observation of in-plane stabilization could be accounted for by the presence of a small amount of C contamination, which was revealed to stabilize perpendicular magnetization surprisingly. Figure 1(b) shows the Ni thickness dependence of the polar MOKE results of Ni/C/Cu(001) before and after Cu capping. In contrast to the Ni films on clean Cu(001), the perpendicular magnetization is apparently unstabilized after Cu capping. The C atoms were found to act as surfactants and were always located at the top surface. As regards perpendicularly magnetized films on clean Cu(001), the enhancement of the coercivity with Cu capping was observed. This finding indicates that Cu does not act as a simple magnetism killer but effectively suppresses the surface anisotropy that favors in-plane magnetic anisotropy.

References

1) W. L. O'Brien and B. P. Tonner, *Phys. Rev. B* **49**, 15370 (1994).

2) H. W. Zhao, Y. Z. Wu, C. Won, F. Toyoma and Z. Q. Qiu, *Phys. Rev. B* **66**, 104402 (2002).

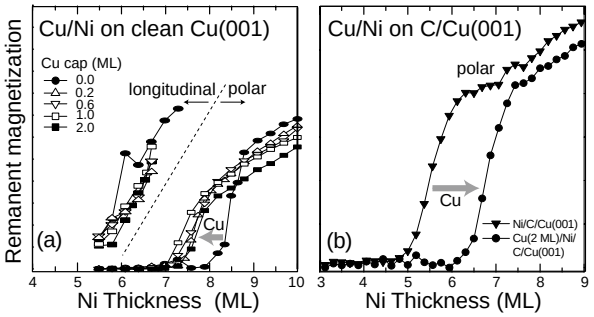

Figure 1. (a) Remanent longitudinal and polar MOKE intensities of Cu-capped Ni films grown on clean Cu(001) as a function of Ni film thickness. The critical thickness of the spin reorientation transition is shifted from ~8.5 ML to a thinner side (~7.5 ML) with increasing the amount of capped Cu. (b) Remanent polar MOKE intensities for Ni films on C-contaminated Cu(001) as a function of Ni film thickness. In contrast to (a), the critical thickness of the spin reorientation transition is shifted from ~5.5 ML to a thicker side (~7.0 M) with Cu capping.

II-F-2 Effect of Surface Chemisorption on the Spin Reorientation Transition in Magnetic Ultrathin Fe Film on Ag(001)

MA, Xiao-Dong[1]; NAKAGAWA, Takeshi; YOKOYAMA, Toshihiko
([1]SOKENDAI)

[*Surf. Sci.* **600**, 4605–4612 (2006)]

We have investigated the effect of surface chemisorption on the spin reorientation transitions in magnetic ultrathin Fe films on Ag(001) by means of the polar and longitudinal MOKE and XMCD measurements. Remanent perpendicular magnetization and the coercive fields of the Fe films on Ag(001) before and

after gas (O_2, NO and H_2) adsorption at 100 K are shown in Figure 1. It is found by the MOKE that adsorption of O_2 and NO induces the shift of the critical thickness for the transitions to a thinner side, together with the suppression of the remanent magnetization and the coercive field of the Fe film. This implies destabilization of the perpendicular magnetic anisotropy. On the other hand, H_2 adsorption is found not to change the magnetic anisotropy, though the enhancement of the coercive field is observed. The XMCD reveals that although both the spin and orbital magnetic moments along the surface normal are noticeably reduced upon O_2 and NO adsorption, the reduction of the orbital magnetic moments are more significant. This indicates that the destabilization of the perpendicular magnetic anisotropy upon chemisorption of O_2 and NO originates from the change of the spin-orbit interaction at the surface.

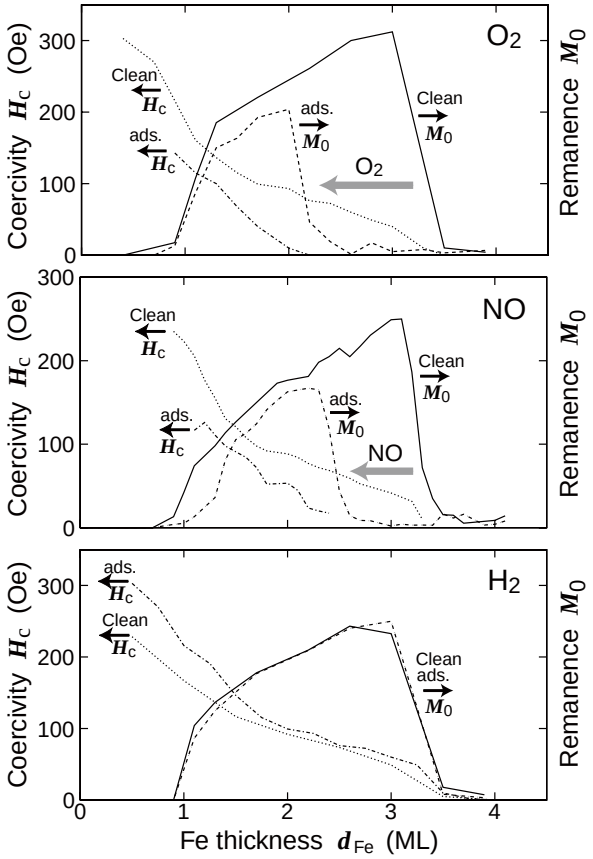

Figure 1. Remanent magnetization and the coercive field of the Fe films on Ag(001) before and after gas (O_2, NO and H_2) adsorption recorded at 100 K by the polar MOKE measurements. O_2 and NO adsorption destabilizes perpendicular magnetic anisotropy, while H_2 does not change the critical thickness.

II-F-3 Magnetic Circular Dichroism near the Fermi Level: Possibility of UV MCD PEEM

NAKAGAWA, Takeshi; YOKOYAMA, Toshihiko

[*Phys. Rev. Lett.* **96**, 237402 (2006)]

It has long been believed that the MCD in the visible and ultraviolet regions is in general too weak to apply for a noble nano-scale magnetic imaging technique of PEEM. In this study, we discovered surprising enhancement of the MCD intensity near the Fermi level using visible and ultraviolet lasers. Figure 1(a) shows the MCD asymmetry of a perpendicularly magnetized Cs-coated 12 ML Ni film on Cu(001) as a function of $h\nu-\Phi$ ($h\nu$ the photon energy and Φ the work function). The work function was changed with the aid of Cs adsorption. More than 10% MCD asymmetry is achieved near the photoemission threshold. The MCD asymmetry is found to be enhanced only near the threshold and to drop down to 0.1% at the photon energy larger than the work function by 0.6 eV. A theoretical calculation also shows enhanced MCD near the photoemission threshold, qualitatively in agreement with the experimental results. Other ultrathin films of 6 ML Ni, 15 ML Co, and 3 and 15 ML Fe on Cu(001) were also investigated. It is found that the perpendicularly magnetized films show much larger MCD asymmetries than the in-plane magnetized films as in the Kerr effect.

Moreover, we have performed the measurements of magnetization curves on clean Ni/Cu(001) using the free electron laser (FEL) from UVSOR-II in order to eliminate the possibilty of the Cs effect. This part is a collaboration with a UVOSR machine group (Prof. M. Kato, Dr. M. Hosaka *et al.*). Figure 1(c) shows the hysteresis loop taken with the photon energy of 5.37 eV. Although the photon energy was not optimized, the MCD asymmetry is found to be as much as 5–6%. This supports the idea that the threshold photoemission provides huge enhanced MCD especially in the perpendicularly magnetized films.

This discovery enables us to exploit a new technique of UV MCD PEEM. At present, x-ray MCD PEEM is widely available for the investigations of nano-scale magnetic imaging of magnetic thin films. This technique however requires third generation synchrotron radiation light sources and cannot be used in laboratories. It is also difficult to obtain information on subpicosecond ultrafast spin dynamics due to the pulse width of the synchrotron radiation. If the UV MCD PEEM techniques can be used in near future, these difficulties can be overcome. We are now developing the new tchnique of UV MCD PEEM.

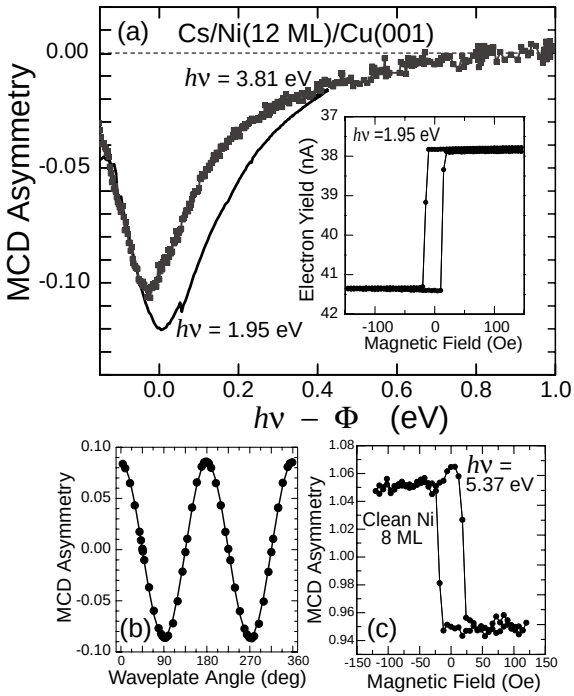

Figure 1. (a) MCD asymmetry from Cs/Ni(12ML)/Cu(001) at normal incidence as a function of $h\nu-\Phi$ ($h\nu$ = 1.95 or 3.81 eV). The work function varied by changing the Cs coverage. The largest MCD asymmetries are as much as 10% near the photoemission threshold. The inset shows the typical magnetization curve. (b) Azimuthal angle dependence of the quarter-wave plate. The angles 0°, 45° and 90° correspond to the left-circularly, linearly, right-circularly polarized lights, respectively. The cosine curve clearly shows the successful bservation of MCD. (c) The magnetization curve of clean Cs-free Ni/Cu(001) taken by using the FEL from UVSOR-II. Intense MCD was observed, eliminating the possibility of the Cs effect for the MCD enhancement.

II-G Development of Fluorescent and Bioluminescent Proteins for Imaging Biomolecules

Our understanding of biological systems is increasingly dependent upon the ability to quantify and image biomolecules in living animals and plants. To probe the biomolecular functions and dynamics in living organisms, we are exploring a new way for developing fluorescent and bioluminescent reporter proteins based on protein splicing. The reporter proteins can be applied to development of analytical methods for detecting protein-protein interactions, intracellular localization of proteins and their dynamics, enzyme activities, gene expression, and production of small bio-molecules. We are also currently investigating analytical techniques such as complementary DNA library screenings and proteome analysis.

II-G-1 A Short Peptide Sequence that Targets Fluorescent and Functional Proteins into the Mitochondrial Intermembrane Space

OZAWA, Takeaki; SAKO, Yusuke[1]; NATORI, Yutaka[1]; KUROIWA, Haruko[2]; KUROIWA, Tsuneyoshi[2]; UMEZAWA, Yoshio[1]
([1]Univ. Tokyo; [2]Rikkyo Univ.)

Protein-based fluorescent and functional probes are widely used for real-time visualization, purification and regulation of a variety of biological molecules. The protein-based probes can generally be targeted into subcellular compartments of eukaryotic cells by a particular short peptide sequence. Little is known, however, about the sequence that targets probes into the mitochondrial intermembrane space (IMS). To identify the IMS-targeting sequence, we developed a simple genetic screening method to discriminate the proteins localized in the IMS from those in the mitochondrial matrix, thereby revealing a sequence sorting into the IMS. An IMS-localized protein, Smac/DIABLO, was randomly mutated and mitochondrial localization of each mutant was analyzed. We found that the four residues of Ala-Val-Pro-Ile are required for the IMS localization, and a sequence of the four residues fused with matrix-targeting signals is sufficient for targeting the Smac/DIABLO in the IMS. The sequence was shown to readily direct multiple proteins of interest to the IMS, which will open avenues to elucidating IMS functions in live cells.

II-G-2 Intein-Mediated Reporter Gene Assay for Detecting Protein-Protein Interactions in Living Mammalian Cells

KANNO, Akira[1]; OZAWA, Takeaki; UMEZAWA, Yoshio[1]
([1]Univ. Tokyo)

[*Anal. Chem.* **78**, 556–560 (2006)]

For nondestructive analysis of chemical processes in living mammalian cells, we developed a new reporter gene assay for detecting cytosolic protein-protein interactions based on protein splicing of transcription factors with DnaE inteins. The protein splicing induces connection of a DNA-binding protein (modified LexA; mLexA) with a transcription activation domain of a herpes simplex virus protein (VP16AD). We thereby circumvented the limitation of earlier methods for monitoring protein-protein interactions, including the two-hybrid systems, protein complementation systems (PCS), and protein reconstitution systems, and rather combined their advantages. To test the applicability of this method, we monitored epidermal growth factor (EGF)-induced interactions on cell membranes of a known partner, an oncogenic product Ras and its target Raf-1. Ras was connected with N-terminal DnaE and mLexA, while Raf-1 was connected with C-terminal DnaE and VP16AD. Upon stimulation with EGF, the interaction between Ras and Raf-1 triggered folding of the DnaEs, thereby inducing protein splicing to form mLexA-VP16AD fusion protein, and transcription of a reporter gene, firefly luciferase. The extent of Ras-Raf-1 interaction was quantified by measuring the luciferase activity. The interaction was not able to be monitored by two-hybrid systems nor by PCS of split firefly luciferases; however, by using the protein splicing elements and the reporter gene, we obtained the bioluminescence signals sufficient for evaluation of the interactions close to cell membranes.

II-G-3 A Genetically Encoded Indicator for Assaying Bioactive Chemicals that Induce Nuclear Transport of Glucocorticoid Receptor

KIM, Sung Bae[1]; OZAWA, Takeaki; UMEZAWA, Yoshio[1]
([1]Univ. Tokyo)

[*Anal. Biochem.* **347**, 213–220 (2005)]

Glucocorticoids, the adrenal steroid hormones secreted during stress, are essential to homeostasis and metabolism in the human body. An impaired glucocorticoid signaling due to dysfunction of the glucocorticoid receptor (GR) by synthetic chemicals can cause diseases and disruptions of the homeostasis and metabolism. Here we demonstrate the development of a method for screening endocrine-disrupting chemicals and potent risk factors of human diseases based on the nuclear trafficking of the GR. We constructed a new assay using a pair of genetic indicators with the full length of the GR, split *Renilla* luciferase (RLuc), and split DnaE (a protein splicing element). The GR-containing fusion protein with C-terminal halves of DnaE and RLuc is localized in cytosol due to the cytosolic character of the GR, whereas the fusion protein with N-terminal halves of DnaE and RLuc stays in the nucleus due to the cofused nucleus localization signal. On being stimulated

with a ligand, the GR is translocated into the cellular nucleus. Thus, the protein splicing occurs in the nucleus by an interaction between the splicing junctions of each DnaE fragment. The enzymatic activities from the reconstituted RLuc allow the ligand-dependent luminescence intensities. The feasibility of the method was evaluated by quantifying the hormonal activities of 20 different kinds of steroids and synthetic chemicals using the NIH 3T3 cells carrying the pair of indicators. The hormonal activities of tested ligands are discussed based on the chemical structure-activity relationship. We found that androgens, testosterone, and 19-nortestosterone weakly induce the nuclear transport of the GR. The current assay allows high-throughput screening of risk chemicals and drug candidates influential to a signal transduction pathway of the GR.

II-G-4 A Method for Determining the Activities of Cytokines Based on the Nuclear Transport of Nuclear Factor-κB

KIM, Sung Bae[1,2]; NATORI, Yutaka[1]; OZAWA, Takeaki; UMEZAWA, Yoshio[1]; TAO, Hiroaki[2]
([1]Univ. Tokyo; [2]AIST)

[*Anal. Biochem.* in press]

Gene expressions are controlled by regulatory proteins known as transcription factors. One important transcription factor is nuclear factor-κB (NF-κB), which is related to cellular proliferation, survival, differentiation, or apoptosis. We developed a method to evaluate the activities of cytokines based on the nuclear transport of NF-κB. A pair of bioluminescent indicators were made for conferring cytokine sensitivity to cervical carcinoma-derived HeLa cells. The principle is based on reconstitution of split fragments of *Renilla* luciferase (RLuc) by protein splicing with a DnaE intein. The bioluminescence intensity of thus reconstituted RLuc in the HeLa cells was used as a measure of the activities for cytokines. The present method would be a useful high-throughput assay for determining the activities of potential biomedical inhibitors on NF-κB trafficking.